J. Biomed. Eng. Res.
Vol. 22, No. 4, 311-319, 2001

A Spline-Regularized Sinogram Smoothing Method for Filtered Backprojection Tomographic Reconstruction

S.J. Lee and H.S. Kim

Department of Electronic Engineering, Paichai University

(Received April 14, 2001. Accepted July 20, 2001)

요 약 : Bayesian 방법을 사용한 통계학적 재구성방법이 방출단층영상에 있어서 중요한 역할을 하여왔는데, 이는 재구성 알고리즘에 복원하고자 하는 영상에 대한 사전정보를 포함시킬 수 있기 때문이다. Bayesian 방법에서는 단층영상의 복원에 대한 수학적 불안정성과 잡음이 내재한 투영 데이터가 주어진 경우 정칙자를 사용하여 적절한 사전정보의 유형을 알고리즘에 포함시킴으로써 해를 안정화시킨다. 본 논문에서는 표준 FBP 알고리즘이 Bayesian 방법에 비해 정량적 차원에서 성능이 떨어지나, 투영데이터 공간에 정칙자를 사용한 평활화 방법을 적용할 경우 FBP 알고리즘도 Bayesian 방법에서 나타나는 유사한 효과와 장점들을 가질 수 있음을 보인다. 이를 위해 우선 정칙화와 저주파통과 필터 의 수학적 관계식을 유도함으로써 정칙자를 사용한 평활 필터의 구현방법을 보인 후 여러 잡음발생을 통해 통계적으로 계산된 bias/variance 및 총제곱오차의 정량적방법을 사용하여 새로운 FBP 방법들의 성능을 비교한다. 정량적 결과에 의하면 3가지 유형의 정칙자 중에서 2차미분항으로 표현되는 정칙자를 사용한 필터를 FBP 알고리즘에 적용할 경우 총제곱오차의 차원에서 최상의 결과를 얻을 수 있다.

Abstract : Statistical reconstruction methods in the context of a Bayesian framework have played an important role in emission tomography since they allow to incorporate *a priori* information into the reconstruction algorithm. Given the ill-posed nature of tomographic inversion and the poor quality of projection data, the Bayesian approach uses regularizers to stabilize solutions by incorporating suitable prior models. In this work we show that, while the quantitative performance of the standard filtered backprojection (FBP) algorithm is not as good as that of Bayesian methods, the application of spline-regularized smoothing to the sinogram space can make the FBP algorithm improve its performance by inheriting the advantages of using the spline priors in Bayesian methods. We first show how to implement the spline-regularized smoothing filter by deriving mathematical relationship between the regularization and the lowpass filtering. We then compare quantitative performance of our new FBP algorithms using the quantitation of bias/variance and the total squared error (TSE) measured over noise trials. Our numerical results show that the second-order spline filter applied to FBP yields the best results in terms of TSE among the three different spline orders considered in our experiments.

Key words : Emission tomography, Image reconstruction, Filtered backprojection, Regularization.

Introduction

The objective of emission computed tomography (ECT) is to determine the three-dimensional (3-D) distribution of radionuclide concentrations within the body using two-dimensional (2-D) projectional views acquired at many different angles about the patient. Therefore, the reconstruction problem in ECT is to compute the distribution of a radionuclide in a given cross section of the human body from the projection measurements. Unfortunately, since the observed data in ECT systems are contaminated by noise due to low count rate and several physical factors, it has been a difficult problem to reconstruct images with good accuracy.

Over the last decade, statistical reconstruction methods [1-8] have enjoyed considerable interest for image reconstruction in ECT since they can accurately model the Poisson noise associated with gamma-ray projection data. In particular, maximum *a posteriori* (MAP) approaches in the context of a Bayesian framework have been a topic of interest since they allow to incorporate a priori information into the reconstruction algorithm. Given the ill-posed nature of tomographic inversion and the poor quality of projection data, Bayesian approaches use regularizers to stabilize solutions by incorporating suitable prior models, which reflect assumptions about the spatial properties of the underlying source distribution. Early methods focused on the regularization of the unstable maximum likelihood (ML) algorithm [1]. Later, the Bayesian approach was also viewed as a means of incorporating actual, known information regarding the

본 연구의 일부는 과학기술부 원자력기초연구사업 및 보건복지부 보건의료기술연구개발사업 (HMP-98-E-1-0008) 지원에 의하여 이루어진 것임.

통신저자 : 이수진, (302-735) 대전시 서구 도마 2동 439-6
배재대학교 전자공학과
Tel.042-520-5711, Fax. 042-520-5773
E-mail. sjlee@mail.pcu.ac.kr

local spatial character of the source. A host of different formulations to model the Bayesian priors have been proposed in the literature [2-7]; some of these implicitly model the underlying radionuclide density as globally smooth [6], and others extend the smoothness model by allowing for spatial discontinuities [2-5,7].

Conventional smoothing priors use quadratic penalties, which are mathematically simple and lead to an algorithm whose solution is easier to compute. However, the conventional quadratic prior, such as the membrane prior, tends to oversmooth discontinuities and incur large bias error. To overcome this problem, we introduced a simple modification of the membrane (MM) prior to one less sensitive to variations in first spatial derivatives - the thin plate (TP) [6], in which Gibbs potentials were applied to spatial second derivative terms better able to model gradual transition regions that separate anatomical boundaries. When the performance of TP was compared with that of MM in terms of quantitation of bias and variance over noise trials using the Monte Carlo method, the TP prior yielded improved reconstruction in the sense of low bias at little change in variance [8]. It was also observed that the use of the TP prior revealed considerably less sensitivity in bias to the variations of smoothing parameter than the MM prior [8].

In this work we note that, while deterministic approaches, such as the filtered backprojection (FBP) method, do not provide as accurate reconstructions as Bayesian methods, the application of spline-regularized smoothing to the sinogram space may lead to quantitatively improved results in FBP reconstruction which is widely used in clinical practice. In this case we may expect the well-known advantages of using the higher-order spline model [5,6] (e.g., the TP prior) in the deterministic FBP method.

In this paper, we first mathematically characterize the relationship between the regularization in Bayesian methods and the lowpass filtering in Fourier-based deterministic methods, and then derive a general form of the nth order angle-independent apodizing filters for FBP reconstruction, which is derived from the nth order smoothing spline models used as priors in Bayesian methods. The remainder of this paper briefly overviews the FBP method in ECT reconstruction, develop a new FBP algorithm with spline-regularized smoothing filters, and presents the results from numerical studies and experiments.

Reconstruction from Projections

Since the physical processes underlying emission tomography are complex, a deterministic solution may not be possible without simplifying assumptions. In the simplest case, the projection can be expressed as a simple line integral or ray sum of the activity distribution along a line which passes through the object. For a 2-D distribution $f(x, y)$ on a single cross-sectional plane, the mathematical expression for the line integral at an arbitrary angle θ is given by

$$g_\theta(t) = \int_{-\infty}^{\infty}\int_{-\infty}^{\infty} f(x, y)\delta(x\cos\theta + y\sin\theta - t)dxdy, \qquad (1)$$

where $g_\theta(t)$ is the ray sum along the line which passes through the object and reaches detector t. Note that $g_\theta(t)$ is a function of t and defines the parallel projection of $f(x, y)$ for angle θ.

A solution of Eq. (1) can be obtained by Fourier slice theorem [9] which relates the one-dimensional (1-D) Fourier transform of a projection of a function $f(x, y)$ to the 2-D Fourier transform of $f(x, y)$:

$$F(\xi, \eta)|_{\xi=\omega\cos\theta, \eta=\omega\sin\theta} = G_\theta(\omega), \qquad (2)$$

where,

$$F(\xi, \eta) = \int_{-\infty}^{\infty}\int_{-\infty}^{\infty} f(x, y)\exp(-2j\pi(\xi x + \eta y))dxdy$$

and

$$G_\theta(\omega) = \int_{-\infty}^{\infty} g_\theta(t)\exp(-j2\pi\omega t)dt.$$

In Eq. (2) $F(\xi, \eta)|_{\xi=\omega\cos\theta, \eta=\omega\sin\theta}$ is the 2-D Fourier transform of $f(x, y)$ evaluated along the line at angle θ, and $G_\theta(\omega)$ is the 1-D Fourier transform of $g_\theta(t)$. If the projections spanned all values of t and θ, the function $f(x, y)$ could be reconstructed by taking the inverse Fourier transform of $F(\xi, \eta)$. In this case, a solution of Eq. (1) is given by

$$f(x, y) = \int_0^{\pi} Q_\theta(x\cos\theta + y\sin\theta)d\theta, \qquad (3)$$

where

$$Q_\theta(t) = \int_{-\infty}^{\infty} G_\theta(\omega)|\omega|\exp(j2\pi\omega t)d\omega \qquad (4)$$

Note that $Q_\theta(t)$ in Eq. (4) is the 1-D inverse Fourier transform of which is the 1-D Fourier transform

$G_\theta(\omega)|\omega|$ of the projection $g_\theta(t)$ filtered by the ramp filter $|\omega|$. In other words, $Q_\theta(t)$ is identified as a "filtered projection". Since any physical system in practice has a practical high-frequency limit, the filter used for filtered projection in Eq. (4) is bandlimited.

Equation (3) can be interpreted in the following way: Every point (x', y'), which contributes to the filtered projection $Q_\theta(t')$ along a line, produces the same value of t' $(=x'\cos\theta+y'\sin\theta)$. Conversely, the filtered projection $Q_\theta(t')$ computed along the line makes the same contribution to all points on the line. Therefore, reconstruction of $f(x, y)$ from the projection $g_\theta(t)$ can be obtained by "smearing" the filtered projection $Q_\theta(t')$ back over the image plane. This reconstruction scheme is identified as Filtered Backprojection (FBP).

Spline-Regularized Sinogram Smoothing

Regularization is a mathematical technique to solve ill-posed problems whose solutions are unstable due to insufficient constraints on the data [10]. The additional constraints to stabilize solutions, termed as "stabilizers" or "regularizers", often take the form of smoothness constraints on possible solutions. Most common approaches to regularization involve finding a minimum of an objective function that consists of a measure of data agreement and a regularizing functional to make the solution well behaved. Given a set of data f which we wish to invert, we define an energy function $E_D(f)$ which measures the closeness of the solution f to the data g. We then add a stabilizing function $E_P(f)$ for smoothness constraints. The regualarization methods thus seek an approximating f which minimizes the following function:

$$E(f)=E_D(f)+\lambda E_P(f),$$

where λ is a positive weight factor that balances between energies $E_D(f)$ and $E_P(f)$. When $E(f)$ is small, f is a good compromise between the data agreement and the smoothness.

Let us consider the p-dimensional space. A common form for the data agreement energy $E_D(f)$ is usually modeled as square error in the fit of $f(\boldsymbol{x})$ to the noisy observation $g(\boldsymbol{x})$:

$$E_D(f)=\int[f(\boldsymbol{x})-g(\boldsymbol{x})]^2 d\boldsymbol{x}$$

where $f(\boldsymbol{x})$ and $g(\boldsymbol{x})$ are defined on the p-dimensional vector space, $\boldsymbol{x}=[x_1,\cdots,x_p]$. The general form of the stabilizers $E_P(f)$ represented by nth-order spline is given by [11]

$$E_P(f)=\int \sum_{m_1+\cdots+m_p=n} \frac{n!}{m_1!\cdots m_p!}\left(\frac{\partial^n f(\boldsymbol{x})}{\partial x_1^{m_1}\cdots\partial x_p^{m_p}}\right)^2 d\boldsymbol{x}, \quad (6)$$

where the value of n determines the order of continuity of the solutions. In the 2-D case, for example, the nth-order spline is reduced to

$$E_P(f)=\int\int \sum_{k=0}^{n}\binom{n}{k}\left(\frac{\partial^n f(x,y)}{\partial x^k \partial y^{n-k}}\right)^2 dxdy.$$

For the two lowest order cases ($n=1$ and $n=2$), the corresponding 2-D spline models are given by

$$E_P(f)=\int\int (f_x^2+f_y^2)dxdy \quad (7)$$

and

$$E_P(f)=\int\int (f_{xx}^2+2f_{xy}^2+f_{yy}^2)dxdy \quad (8)$$

for $n=1$ and $n=2$, respectively. Based on the physical interpretations in elasticity theory [11,12], these cases can be explained in the following way. For $n=1$, Eq. (7) represents the small deflection energy of a "membrane". For $n=2$, Eq. (8) corresponds to the small deflection bending energy of a "thin plate".

Below, we investigate the mathematical relationship between the regularization and the lowpass filtering. Since regularizers typically take the form of space-invariant smoothness constraints, we may regard the regularization as smooth filtering or lowpass filtering with a corresponding Fourier domain representation. To see the spectral properties of energy function solutions, we may use a Fourier analysis. The Fourier transform of a multidimensional signal $s(\boldsymbol{x})$ is defined by

$$S(\boldsymbol{\omega})=\mathcal{F}\{s(\boldsymbol{x})\}=\int_{-\infty}^{+\infty} s(\boldsymbol{x})\exp(-j2\pi\,\boldsymbol{\omega}\cdot\boldsymbol{x})d\boldsymbol{x}$$

and the Fourier transform of its partial derivative with respect to the ith compoment of $\boldsymbol{x}$, x_i, is given by

$$\mathcal{F}\left\{\frac{\partial s(\boldsymbol{x})}{\partial \boldsymbol{x}_i}\right\}=-j2\pi k_i S(\boldsymbol{\omega}), \quad (9)$$

where ω_i is the ith component of $\boldsymbol{\omega}$. Using Parseval's Theorem,

$$\int_{-\infty}^{+\infty}|s(\boldsymbol{x})|^2 d\boldsymbol{x}=\int_{-\infty}^{+\infty}|S(\boldsymbol{\omega})|^2 d\boldsymbol{\omega},$$

and Eq. (9), we may rewrite Eqs. (5) and (6) as

$$E_D(f)=\int_{-\infty}^{+\infty}|f(\boldsymbol{x})-g(\boldsymbol{x})|^2 d\boldsymbol{x}=\int_{-\infty}^{+\infty}|F(\boldsymbol{\omega})-G(\boldsymbol{\omega})|^2 d\boldsymbol{\omega}$$

and

$$E_P(f)=\int_{-\infty}^{+\infty}\sum_{m_1+\cdots+m_p=n}\frac{n!}{m_1!\cdots m_p!}\left|\frac{\partial^n f(\boldsymbol{x})}{\partial x_1^{m_1}\cdots\partial x_p^{m_p}}\right|^2 d\boldsymbol{x}$$

$$=\int_{-\infty}^{+\infty}\sum_{m_1+\cdots+m_p=n}\frac{n!}{m_1!\cdots m_p!}|(j2\pi\omega_1)^{m_1}\cdots(j2\pi\omega_p)^{m_p}F(\boldsymbol{\omega})|^2 d\boldsymbol{\omega}$$

$$=\int_{-\infty}^{+\infty}|2\pi\boldsymbol{k}|^{2n}|F(\boldsymbol{k})|^2 d\boldsymbol{k},$$

respectively. Hence, the overall energy $E(f)$ is given by.

$$E(f)=\int_{-\infty}^{+\infty}[\,|F(\boldsymbol{\omega})-G(\boldsymbol{\omega})|^2+\lambda|2\pi\boldsymbol{\omega}|^{2n}|F(\boldsymbol{\omega})|^2]d\boldsymbol{\omega}$$

$$=\int_{-\infty}^{+\infty}[\,(1+\lambda|2\pi\boldsymbol{\omega}|^{2n})|F(\boldsymbol{\omega})|^2-2|G(\boldsymbol{\omega})||F(\boldsymbol{\omega})|+|G(\boldsymbol{\omega})|^2]d\boldsymbol{k}$$

The above energy is minimum when $F(\boldsymbol{\omega})=\hat{F}(\boldsymbol{\omega})$, where $\hat{F}(\boldsymbol{\omega})$ is given by

$$\hat{F}(\boldsymbol{\omega})=\frac{1}{(1+\lambda|2\pi\boldsymbol{\omega}|^{2n})}G(\boldsymbol{\omega})$$

Let $H(\boldsymbol{\omega})=\hat{F}(\boldsymbol{\omega})/G(\boldsymbol{\omega})$. Then we have

$$H(\boldsymbol{\omega})=\frac{1}{(1+\lambda|2\pi\boldsymbol{\omega}|^{2n})} \tag{10}$$

Notice that Eq. (10) takes the form of a lowpass filter, where λ controls the bandwidth of the filter. The larger the value of λ, the narrower the filter bandwidth, thereby weighting the smoothing effect more strongly.

It is important to point out here that the origin of the above lowpass filter is in the nth-order smoothing spline models described in Eq. (6) and that the filter may be incorporated into the FBP algorithm in the form of a simple linear apodizing filter. In the sinogram space, the lowpass filtering is equivalent to taking a convolution with the inverse Fourier transform of Eq. (10), which eventually is equivalent to smoothing the sinogram using the spline model specified in Eq. (6). In this case we may expect similar effects of using the smoothing spline models as priors in Bayesian methods.

Recall that, in FBP reconstruction, the filtered projection $Q_\theta(t)$ in Eq. (4) is the 1-D inverse Fourier transform of $G_\theta(\omega)|\omega|$, where the Fourier transform of the projection, $G_\theta(\omega)$, is filtered by the ramp filter $|\omega|$. In fact, since the filter in Eq. (4) is a convenient place to accomplish the overall system filtering in addition to the basic $|\omega|$ filtering, a wide variety of filter functions are used in practice. These filters generally involve the product of $|\omega|$ and a high-frequency apodizing filter in order to suppress the noise amplification in high frequencies as well as to moderate the abrupt truncation of the ramp filter which causes "ringing" at the edges in the reconstructed image. In this paper, instead of using conventional lowpass filters, such as Hamming or Hanning windows, we combine the spline-regularized smoothing filter described in Eq. (10) with the ramp filter. In this case high-frequency apodization in FBP is implemented in the Fourier domain of the projection data using the angle-independent apodizing filters that multiply the ramp filter. We also point out that unapodized FBP reconstructions ($\lambda=0$) were far worse than the apodized versions in all cases, so no such results are reported.

Experimental Results

To test our idea of using the spline-regularized smoothing filter for FBP reconstruction, we performed 2-D simulation studies with projection data from 128×128 digital phantoms, designated A and B for convenience, with 128 projection angles over 180° and 128 detector bins at each projection. Phantom A (Fig. 1(a)) is a digital Hoffman brain phantom with activity of 4:1:0 in grey matter, white matter, and CSF, respectively. Phantom B (Fig. 1(b)) was derived from a digitized

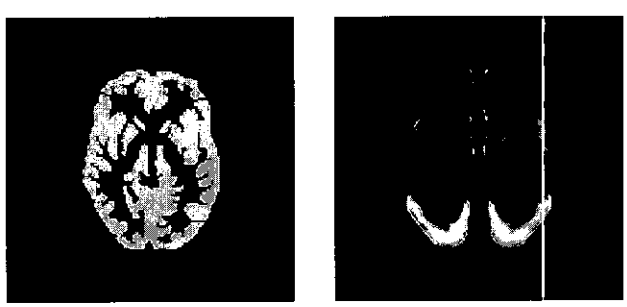

(a) (b)

Fig. 1. Digital phantoms used in the experiments. (a) Hoffman brain phantom A. (b) Autoradiograph phantom B.

rhesus monkey autoradiograph [13]. The motivation of using such a phantom is based on our hypothesis that biologically realistic phantoms are useful in testing reconstruction algorithms for emission tomography [5-8].

In this work, we compared quantitative performance of the spline-regularized smoothing filters in Eq. (10) for three different orders ($n=1$, 2, and 3). Since the results from anecdotal, single-image comparisons are not convincing in medical imaging, we evaluated the reconstructions in an ensemble sense; we first generated 50 Monte Carlo noise trials for each phantom by adding independent realizations of Poisson noise to the noiseless projection data. For each set of noisy projection data, we then performed FBP reconstructions with the three different spline orders. Since the quality of reconstructions depends highly on the smoothing parameter λ, instead of choosing and fixing the value of λ, we used a range of values; for phantom A, we used $\lambda_i=0.025\times 2^i$, and for phantom B, $\lambda_i=0.05\times 2^i$, where $i=0, 1, 2, \cdots, 8$. Thus the total number of reconstructions performed for each phantom was 1,350 (50 noise realizations, 9 values of λ, 3 values of n).

To evaluate the reconstructions quantitatively, we computed bias and standard deviation (STD) images. A bias image, b_{ij}, is defined as

$$b_{ij}=\frac{1}{K}\sum_{k=1}^{K}(\hat{f}_{ij}^{k}-f_{ij}), \tag{11}$$

where $\hat{f}_{ij}^{k}$ is the kth reconstruction of phantom f at location (i,j) and the summation is over $K=50$ independent noise trials. To display the bipolar bias image, an intermediate grey scale value of 128 out of 256 levels was used as zero bias. A standard deviation image, s_{ij}, is defined as

$$s_{ij}=\sqrt{\frac{1}{K-1}\sum_{k=1}^{K}(\hat{f}_{ij}^{k}-\bar{f}_{ij})^2}, \tag{12}$$

where $\bar{f}_{ij}$ is the mean of $\hat{f}_{ij}$ over noise trials. We also computed the total squared error (TSE) t^2 defined as

$$t^2=\sum_{ij}(b_{ij}^2+s_{ij}^2), \tag{13}$$

which summarizes the bias and STD results.

Figure 2 shows anecdotal reconstructions for both phantoms A and B, where (a)(d), (b)(e), and (c)(f) are for

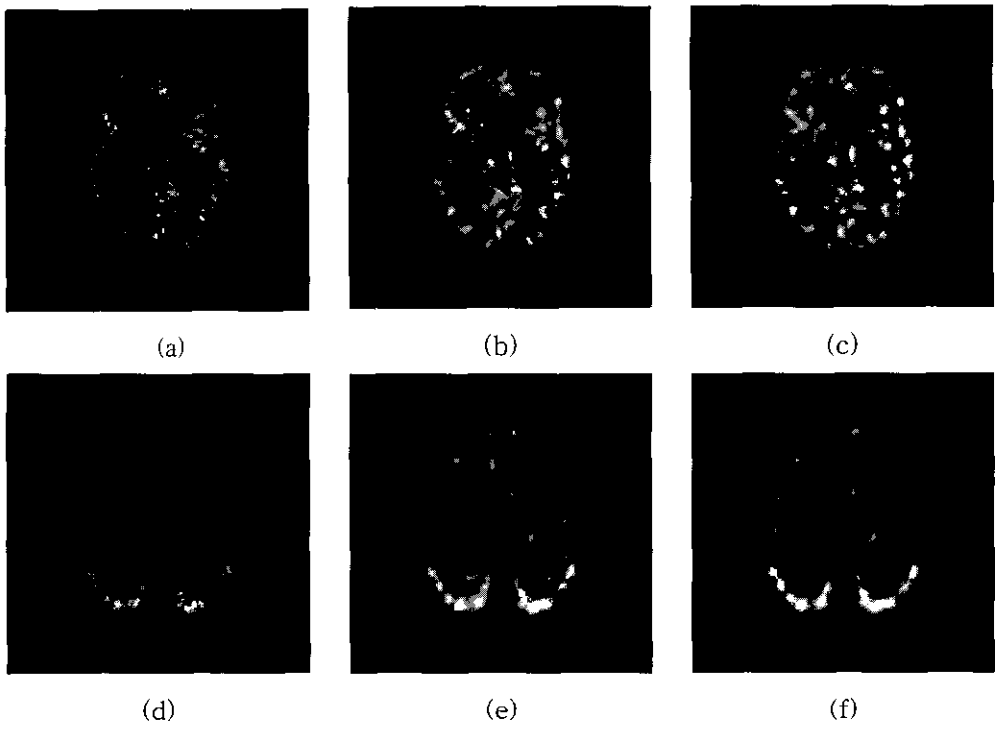

Fig. 2. Anecdotal FBP reconstructions for phantoms A ((a)-(c)) and B ((d)-(f)). (a) $n=1$. (b) $n=2$. (c) $n=3$. (d) $n=1$. (e) $n=2$. (f) $n=3$.

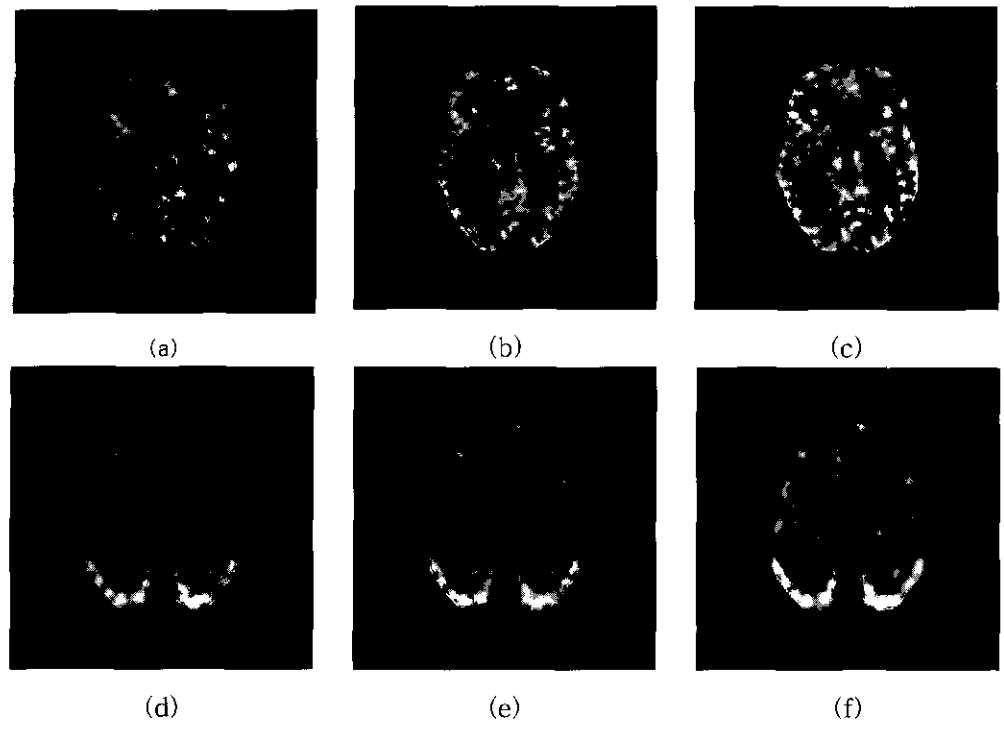

Fig. 3. Conventional FBP and Bayesian reconstructions for phantoms A ((a)-(c)) and B ((d)-(f)). (a) FBP with Hanning window (b) Bayesian with MM prior. (c) Bayesian with TP prior. (d) FBP with Hanning window. (e) Bayesian with MM prior. (f) Bayesian with TP prior.

$n=1$, 2, and 3, respectively. In Fig. 2 the value of λ was chosen by finding the value that yielded the smallest TSE over a range. Therefore, the images in Fig. 2 are the best anecdotal results in terms of TSE. Close inspection reveals that the reconstruction using $n=2$ captures subtle aspects of each phantom better than other cases ($n=1$ or 3). Comparisons of (a)(d) to (c)(f) show that increasing the spline order appears to increase the degree of smoothness. This is presumably due to the fact that, when viewed as a 2-D regularization problem, the higher the differential order, the larger the number of pixels participating in the regularization. For example, while the membrane model ($n=1$) in Eq. (7) uses 4 nearest pixels, the thin plate model ($n=2$) in Eq. (8) uses 12 nearest pixels. However, it is important to point out here that the effect of increasing the spline order n is different from that of increasing the value of λ in that changing the value of λ does not change the number of pixels in the neighborhood of a pixel to be updated. The details on the cross effect due to λ and n can be found in the experimental results from our quantitative performance test.

Since our smoothing filters are based on the spline priors used for Bayesian methods and applied to FBP, for qualitative comparison purposes, we also include some representative reconstructions obtained from the Bayesian method with simple spline priors and a conventional FBP reconstruction. As shown in Figs. 3(a) and (d), the conventional FBP method, which uses a Hanning window for high-frequency apodization, tends to oversmooth the entire image area by ignoring local spatial characteristics of the underlying source. On the other hand, it is clearly shown in Figs. 3 (b), (c), (e), and (f) that the Bayesian method significantly improves the quality of reconstructions. (The details on the quantitative performance of the Bayesian method used for these results can be found in our previous publications [6,8].) Note also that the transitions from Figs. 3(b) and (e) to (c) and (f), respectively, in Bayesian reconstructions are similar to those from Figs. 2(a) and (d) to (b) and (e), respectively. This qualitatively shows that the use of spline regularized smoothing filters for high frequency apodization makes the FBP algorithm improve its performance by inheriting the advantages of using the spline priors in Bayesian methods.

Figure 4 shows the total squared error t^2 versus the smoothing parameter λ for FBP reconstructions using our spline-regularized smoothing method. Notice that the

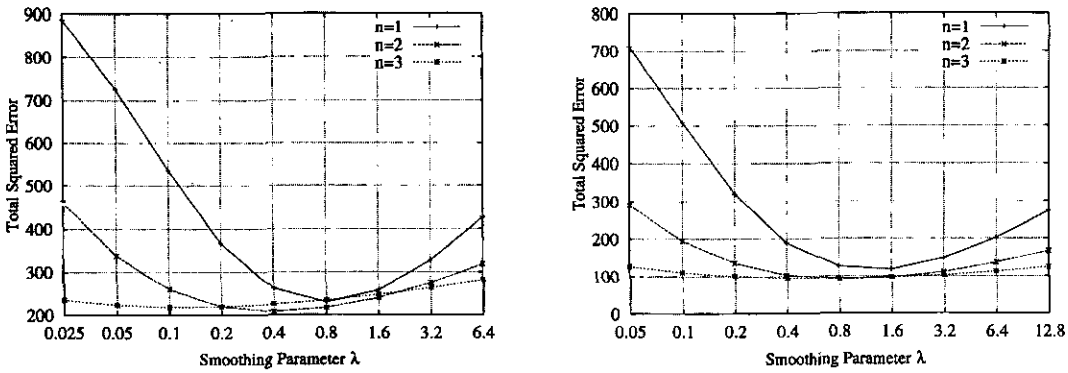

Fig. 4. Total squared error t^2 versus smoothing parameter λ for three different spline orders ($n=1, 2$, and 3). (a) Phantom A. (b) Phantom B.

ranges of λ considered in our experiments are realistic in that, for each order n, the value of λ that yields a minimum of t^2 is near the center of the range. The curves in Fig. 4 indicate that the higher the order n, the less the sensitivity of the smoothing spline filter to the variations of λ. In fact, while all of the curves in Fig. 4 are unimodal over a wide range of λ, the curves for $n=3$ turns out to be least sensitive to the variations of λ for both phantoms A and B. This indicates that the use of higher-order models can alleviate the problem of choosing the smoothing parameter by allowing a wide range for the value of λ.

According to our experimental results, the major source of characterizing the TSE curve (Fig. 4) of a spline filter is the bias error rather than the STD error. Figures 5 and 6 show the pointwise bias images for phantoms A and B, respectively, where the results from the three different values of λ ($\lambda_0, \lambda^*, \lambda_8$) for each spline order are shown. In Figs. 5 and 6, λ^* is the value of the smoothing parameter that yields the smallest TSE. The pointwise bias images clearly show that, as the spline order n increases, the sensitivity of bias error to the

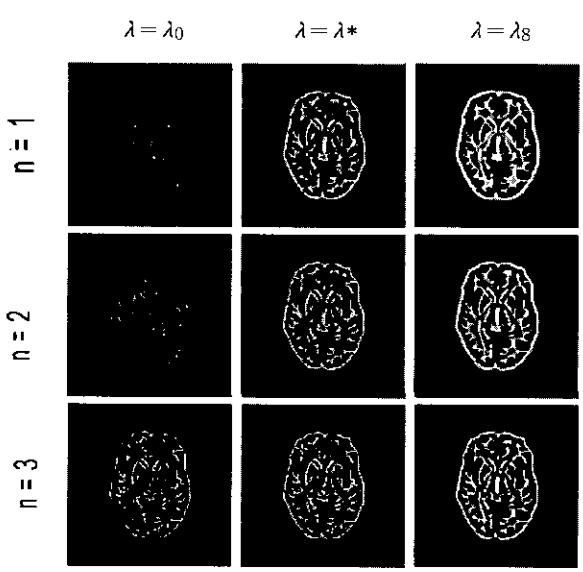

Fig. 5. Pointwise bias images for phantom A obtained from 50 independent noise realizations. The bias images are bipolar, with a value of zero displayed as an intermediate grey, with darker/lighter regions corresponding to negative/positive bias

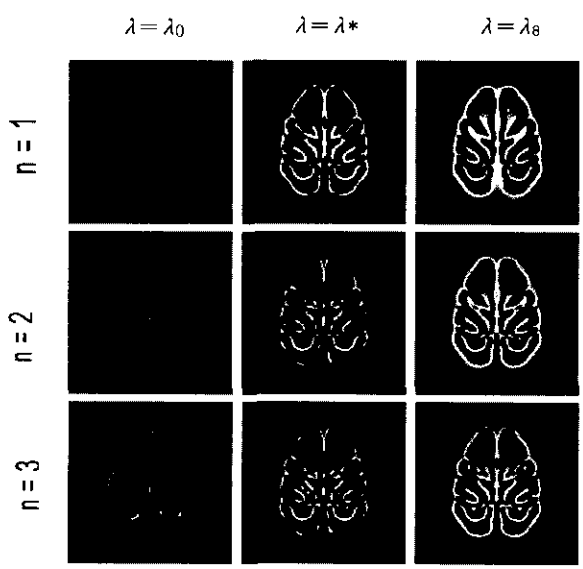

Fig. 6. Pointwise bias images for phantom B obtained from 50 independent noise realizations

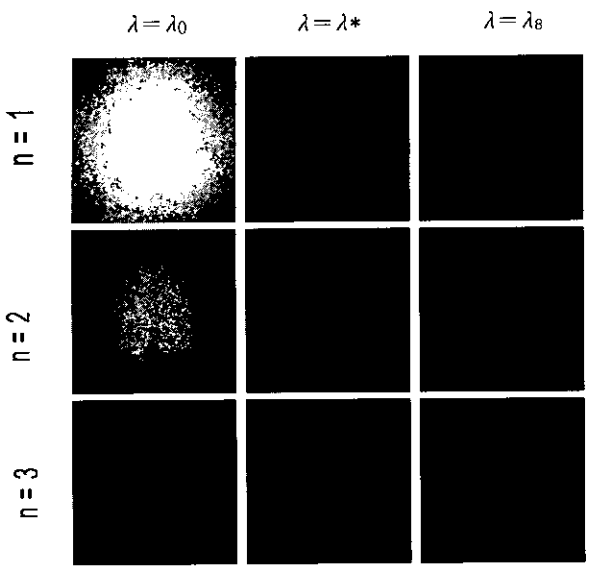

Fig. 7. Pointwise STD images for phantom B obtained from 50 independent noise realizations

variations of λ decreases. For instance, the change of the contrast in the bias images from λ_0 to λ_8 for $n=1$ is much larger than that for $n=3$.Figure 7 shows the pointwise STD images for phantom B. (Since the results from phantom A are visually similar to those from phantom A, they are not reported here.) Note that the same grey scale normalization was used for all images to allow fair comparisons. Similarly to the results for the pointwise bias images, the sensitivity of STD error to the variations of λ decreases as the spline order n increases.

The results in Figs. 4 to 7 show the usual bias/variance tradeoff; large values of λ lead to larger bias but smaller variance, and the opposite is true for small values of λ. In order to obtain the quantitatively best result, it is necessary to choose λ that yields the smallest errors in both bias and variance.

Table 1 summarizes the smallest TSEs and the corresponding optimal values of λ (λ^*) for each order of the spline filter. Note that, although the sensitivity of a spline filter to the variations of λ in terms of TSE decreases as the order n increases, the smallest TSE is minimal (207.70 and 92.46 for phantoms A and B, respectively) at the second order ($n=2$). This implies that increasing the order does not always improve the quality of reconstructions. According to our experimental results, the use of high spline orders above $n=2$ tends to oversmooth reconstructed images. This is presumably due to the fact that a high order spline filter above $n=2$ has the effect of using a large number of pixels for regularization, which may in turn degrade the resolution of reconstructed images by using many pixels far from the pixel of interest.

Table 1. The smallest TSEs (t^2)and corresponding λ (λ^*)

Order	Phantom A		Phantom B	
	λ^*	t^2	λ^*	t^2
$n=1$	0.8	229.93	1.6	117.94
$n=2$	0.4	207.70	0.8	92.46
$n=3$	0.1	218.06	0.8	93.69

Summary and Conclusion

We have considered a spline-regularized sinogram smoothing method for FBP reconstruction. The method is based on the mathematical relationship between the regularization and the lowpass filtering. In this case, although the quantitative performance of the standard FBP algorithm is not as good as that of Bayesian methods, the simpler FBP algorithm with spline filters provides the well-known advantages of using higher order regularizers, such as the thin-plate prior, in Bayesian methods.

The results from our quantitative performance test show that the higher the spline order, the less sensitive the spline filter in both bias and variance to the variations of the smoothing parameter, which indicates that the use of higher order filters can alleviate the problem of choosing the smoothing parameter λ. However, the quantitative results also show that increasing the order does not always improve the quality of reconstructions in that, above some orders, the minimum TSE increases as the spline order increases. Therefore, it is necessary to choose a proper order to achieve the quantitatively best result. According to our simulation results, the second order ($n=2$) yielded a minimum in TSE.

The net conclusion is that, while the quantitative performance of the deterministic FBP algorithm is known to be poor compared to that of Bayesian methods, the use of spline regularized smoothing filters for high frequency apodization makes the FBP algorithm improve its performance by inheriting the advantages of using the spline priors in Bayesian methods.

REFERENCES

1. Shepp and Y. Vardi, "*Maximum Likelihood Reconstruction for Emission Tomography*", IEEE Trans. Med. Imaging, 1, pp. 113-122, 1982
2. T. Hebert and R. Leahy, "*A Generalized EM Algorithm for 3-D Bayesian Reconstruction for Poisson Data Using Gibbs Priors*", IEEE Trans. Med. Imaging, 8(2), pp. 194-202, 1989
3. P.J. Green, "*Bayesian Reconstructions from Emission Tomography Data Using a Modified EM Algorithm*", IEEE Trans. Med. Imaging, MI-9(1), pp. 84-93, 1990
4. D.S. Lalush and B.M.W. Tsui, "*A Generalized Gibbs Prior for Maximum A Posteriori Reconstruction in SPECT*", Phys. Med. Biol., 38, pp. 729-741, 1993
5. S.J. Lee, A. Rangarajan, and G. Gindi, "*Bayesian Image Reconstruction in SPECT Using Higher Order Mechanical Models as Priors*", IEEE Trans. Med. Imaging, 14(4), pp. 669-680, 1995
6. S.J. Lee, I.T. Hsiao, and G.R. Gindi, "*The Thin Plate as a Regularizer in Bayesian SPECT Reconstruction*", IEEE Trans. Nuclear Science, 44(3), pp. 1381-1387, 1997
7. S.J. Lee, Y. Choi, and G. Gindi, "*Validation of New Gibbs Priors for Bayesian Tomographic Recon struction Using Numerical Studies and Physically Acquired Data*", IEEE Trans. Nuclear Science, 46(6), pp. 2154-2161, 1999
8. S.J. Lee, I.T. Hsiao, G.R. Gindi, "*Quantitative Effects of Using Thin-Plate Priors in Bayesian SPECT Reconstruction*", In Proc. SPIE: Image Reconstruction and Restoration II, 3170, pp.252-263, July 1997
9. G.T. Herman, Image Reconstruction from Projections, Academic Press, New York, NY, 1980
10. A.N. Tikhonov and V.Y. Arsenin, Solution of Ill-Posed Problems, Winston and Wiley, Washington D.C., 1977
11. D. Terzopoulos, "*Regularization of Inverse Visual Problems Involving Discontinuities*", IEEE Trans. Patt. Anal. Mach. Intell., 8, pp. 413-424, July 1986
12. D. Terzopoulos, "*Multilevel Computational Processes for Visual Surface Reconstruction*", Computer Vision, Graphics, and Image Processing, 24, pp. 52-96, 1983
13. J.L. Lear, "*Principles of Single and Multiple Radionuclide Autoradiography*", In M.E. Phelps, J.C. Mazziotta, and H.R. Schelbert, editors, Positron Emission Tomography and Autoradiography, Chapter 5, Raven Press, New York, NY, 1986